

# The Energy Cost of Artificial Intelligence Lifecycle in Communication Networks

Shih-Kai Chou<sup>1</sup>, Jernej Hribar<sup>1</sup>, Vid Hanžel<sup>1</sup>, Mihael Mohorčič<sup>1</sup>, Carolina Fortuna<sup>1</sup>

**Abstract**—Artificial Intelligence (AI) is being incorporated in several optimization, scheduling, orchestration as well as in native communication network functions. This paradigm shift results in increased energy consumption, however, quantifying the end-to-end energy consumption of adding intelligence to communication systems remains an open challenge since conventional energy consumption metrics focus on either communication, computation infrastructure, or model development. To address this, we propose a new metric, the Energy Cost of AI Lifecycle (eCAL) of an AI model in a system. eCAL captures the energy consumption throughout the development, deployment and utilization of an AI-model providing intelligence in a communication network by (i) analyzing the complexity of data collection and manipulation in individual components and (ii) deriving overall and per-bit energy consumption. We show that as a trained AI model is used more frequently for inference, its energy cost per inference decreases, since the fixed training energy is amortized over a growing number of inferences. For a simple case study we show that eCAL for 100 inferences is 2.73 times higher than for 1000 inferences. Additionally, we have developed a modular and extendable open-source simulation tool to enable researchers, practitioners, and engineers to calculate the end-to-end energy cost with various configurations and across various systems, ensuring adaptability to diverse use cases.

**Index Terms**—AI Model lifecycle, Energy Consumption, Carbon Footprint, Metric, Methodology

## I. INTRODUCTION

Next-generation wireless networks aim to deliver unprecedented levels of connectivity, service diversity and flexibility. Artificial Intelligence (AI) is expected to become fundamental to 6G and future cellular networks [1], with traditional networking functions increasingly being supplanted by AI-driven implementations to realize so-called “AI-native” capabilities [2], [3]. These AI techniques aim to deliver intelligent, sustainable, and dynamically programmable services that enhance network adaptability and flexibility [1]. Recent works propose a pervasive multi-level native AI architecture that incorporates knowledge graph (KG) into mobile network reducing data scale and computational costs of AI training by almost an order of magnitude [4], attempt to improve communication network efficiency by minimizing the transmitted data through semantic communications [5], and optimize end-to-end network slicing [6]. Furthermore, and AI/Machine Learning (ML) workflow was defined [7] as part of the Open Radio Access Network (O-RAN) Alliance that tackles the standardization of the network access segment.

While such systems designed through endogenous AI models enable unprecedented automation and agility as well as

improved energy consumption for the performed data transmission, their reliance on AI implies additional energy consumption and increased carbon emissions [8]. These energy and carbon costs may be significant [9], especially in the cases where models with many parameters are employed, such as large language models (LLMs). Projections indicate that by 2030, electricity consumption could rise to 100 TWh for data centers and 40 TWh for telecommunication networks [10].

In light of climate challenges, the general AI research community’s efforts are intensifying. They aim to better estimate the costs of training [11] and using AI [12], assess the Carbon Footprint (CF) of LLMs [13], and find ways to scale models efficiently [14]. Furthermore, while increasingly relying on AI techniques, the networking community is also exploring pathways towards net-zero carbon emissions [15]. In particular, researchers analyze the CF of different learning techniques [16] and data modalities and develop different approaches to optimize energy efficiency, including joint optimization of hardware-software co-design [17], improved scheduling [18], more efficient model design [19], and energy/carbon consumption testing [20].

Depending on the scope of the study, various metrics are employed to understand energy efficiency (EE) and CF. As well noted in [15], the traditional ITU standardized Energy-per-Bit [ $J/b$ ] metric ‘will no longer be able to reflect the environmental impact of the modern mobile services, especially network AI-enabled smart services’. For instance, [17] considers both normalized energy and energy for buffering (in [ $J$ ]), whereas [15], [16] examine electricity consumption (in [ $Wh$ ]) and carbon emissions (in [ $CO_2eq$ ]) for the various phases involved in federated learning (FL) edge systems. The energy cost and computational complexity ( $[J]$  and GFLOPS) of neural architectures are evaluated in [19], while [18] focuses on energy cost [ $Wh$ ] of scheduled loads. However, *these metrics are not specifically designed to capture the EE of a system or its parts*. To this end, a metric somewhat similar to the Energy-per-Bit [ $J/b$ ] would be more suitable for measuring EE of an AI-based communication system, similarly as some other efficiency metrics that have been proposed in wireless systems in particular and in engineering and economy in general [21]. For instance, spectral efficiency, measured in [ $b/s/Hz$ ] [22] provides means of calculating the amount of data bandwidth available in a given amount of spectrum, and lifecycle emissions for vehicles, measured in [ $g/km$ ] [23], enable computing the CF in grams per kilometer.

Following these observations, we tackle a timely, unexplored and complex problem aimed to find a suitable EE

<sup>1</sup>Jožef Stefan Institute, Ljubljana, 1000, Slovenia. Corresponding author: Shih-Kai Chou (e-mail: shih-kai.chou@ijs.si)

metric that would be simple and general and would holistically quantify the environmental cost of inference carried out in future communication networks. This work is meant as the foundation on which to build increasingly accurate understanding of the cost of AI model embedding in networks. The contributions of this paper are as follows:

- We propose a new metric, the Energy Cost of AI Lifecycle (eCAL), measured in  $[J/b]$ , that captures the overall energy cost of generating an inference in a communication system. Unlike capturing the energy required for transmitting bits that is done by the Energy-per-Bit  $[J/b]$  metric, or  $[J]$  for AI model complexity, the proposed eCAL captures the energy consumed by all the data collection and manipulation components in an AI-enhanced system during the lifecycle of a trained model delivering inference.
- Following the standard Open Systems Interconnection (OSI) model and AI/ML workflow or Machine Learning Operations (MLOps) [24], falling under the platform layer of the standard Cloud Computing Reference Architecture (CCRA), we devise a methodology for determining the eCAL of an communication system and develop an open source modular and extensible eCAL calculator<sup>1</sup>. The methodology breaks down the system into different data manipulation components, and, for each component, it analyzes the complexity of data manipulation and derives the overall energy consumption.
- Using the proposed metric, we demonstrate that the better a model and the more it is used, the more energy-efficient is inference. For a selected case study, the energy consumption per bit for 100 inferences is 2.73 times higher than for 1000 inferences. This can be explained by the fact that the energy cost of data collection, preprocessing, training, and evaluation, all necessary to develop an AI model, are spread across more inferences.

The paper is organized as follows. Section II reviews related work. Section III describes the AI model lifecycle, introduces eCAL, and outlines its derivation methodology. Sections IV–VII present energy consumption formulas for the data manipulation components of the lifecycle. Section VIII derives and analyzes eCAL for selected communication and model development cases, illustrating its effectiveness in capturing overall lifecycle energy costs. Section IX concludes the paper and discusses future research directions.

## II. RELATED WORK

*AI Environmental Impact:* The growing dependence on AI has introduced significant energy and carbon costs [8], intensifying environmental concerns [13]. In response, the AI research community has placed greater emphasis on understanding and then formalizing methods to assess the environmental impact of the increasing AI adoption. Due to the complexity of state-of-the-art neural network architectures, in many cases the energy cost of training is computed after the

training is done, by measuring the performed computation through interfaces such as the performance application programming interface [25]. Furthermore, [11] showed that *the energy footprint of inference has been more extensively studied than that of training*. The study highlighted that the accuracy between the predicted and measured energy consumption is below 70%.

*Emerging in the AI Community:* A number of approaches and tools capable of proactively estimating the energy and environmental cost of training have also emerged. LLMCarbon [13] is a very recent end-to-end CF projection model designed for both dense (all parameters are used for every input) and mixture of experts (only a subset of parameters for each input) LLMs. It incorporates critical LLM, hardware, and data center parameters, such as LLM parameter count, hardware type, system power, chip area, and data center efficiency, to model both operational and embodied CFs of an LLM. Furthermore, [14] aimed to provide guidelines for scaling AI in a sustainable way. They examined the EE of new processing units and the CF of the most prominent LLM models since GPT-3, analyzed their lifecycle carbon impact, and showed that inference and training are comparable. They concluded that to enable sustainability as a computer system design principle, better tools for carbon telemetry, large-scale carbon datasets, carbon impact disclosure, and more suitable carbon metrics are required.

*Emerging in the Networking Community:* Increasingly relying on AI techniques, the networking community is also investigating pathways towards net-zero carbon emissions [15]. In [15] the authors noticed that in spite of improvements in hardware and software energy efficiency, the overall energy consumption of mobile networks continues to rise, exacerbated by the growing use of resource-intensive AI algorithms. They introduced a novel evaluation framework to analyze the lifecycle of network AI implementations, identifying major carbon emission sources. They proposed the dynamic energy trading and task allocation framework, designed to optimize carbon emissions by reallocating renewable energy sources and distributing tasks more efficiently across the network. Similar to [14], they highlighted the need for the development of new metrics to quantify the environmental impact of new network services enabled by AI.

The authors of [16] introduced a novel framework to quantify energy consumption and carbon emissions for vanilla FL methods and consensus-based decentralized approaches, and identified optimal operational points for sustainable FL designs. Two case studies were analyzed within 5G industry verticals: continual learning and reinforcement learning scenarios. Similar to the authors of [15], they considered energy  $[Wh]$  and carbon emissions  $[CO_2eq]$  in their evaluations. The solution proposed in [17] is a hardware/software co-design that introduces modality gating (throttling) to adaptively manage sensing and computing tasks. It features a novel decoupled modality sensor architecture that supports partial throttling of sensors, significantly reducing energy consumption while maintaining data flow across multimodal data: text, speech,

<sup>1</sup><https://github.com/sensorlab/eCAL>

TABLE I: State-of-the-art energy efficiency metrics, their relevance across the AI lifecycle, and additional system context.

Column	(2)	(3)	(4)	(5)	(6)	(7)	(8)	(9)	(10)	(11)
Characteristic	Metrics									
	Energy Efficiency	Energy per Bit	PUE	CUE	WUE	APC	APEC	TTCAPC	TTCAPEC	eCAL
Category	Telecom	Telecom	Data Center	Data Center	Data Center	Deep Learning	Deep Learning	Deep Learning	Deep Learning	Proposed
Units	$b/J$	$J/b$	%	$kg/kWh$	$L/kWh$	%	%	%	%	$J/b$
Description	Measures information bits per Joule consumed by the radio access network or communication module.	Energy consumed to transmit one bit over the link.	Power Usage Effectiveness: ratio of total facility energy to energy delivered to IT.	Carbon Usage Effectiveness: CO <sub>2</sub> ( $kg$ ) per kWh consumed.	Water Usage Effectiveness: liters of water per kWh for cooling/operation.	Accuracy per Consumption: accuracy relative to the energy cost of model weights (GreenAI).	Accuracy per Energy Cost: variant of APC capturing broader costs.	Time to Closest APC: integrates training time and energy into APC.	Time to Closest APEC: integrates training time and energy into APEC.	End-to-end energy of AI data collection/inference relative to application bits (comms + compute).
<b>Mapping to the telco OSI standard layers and cloud computing CCRA standard layers.</b>										
OSI Standard	Physical	Physical	All	All	All	Application	Application	Application	Application	All
CCRA Standard	$\times$	$\times$	All	All	All	Service	Service	Service	Service	Service, Platform
<b>Relevance to the data-manipulating components in the AI lifecycle</b>										
Data Collection (Sec. IV)	✓	✓	✓	✓	✓	✗	✗	✗	✗	✓
Preproc. (Sec. V)	✗	✗	✓	✓	✓	✗	✗	✗	✗	✓
Training (Sec. VI)	✗	✗	✓	✓	✓	✓	✓	✓	✓	✓
Evaluation (Sec. VII)	✗	✗	✓	✓	✓	✓	✓	✓	✓	✓
Inference (Sec. VIII)	✗	✗	✓	✓	✓	✓	✓	✗	✗	✓

images, and video. More energy efficient task scheduling has been considered in [18], while more efficient neural network architecture design and subsequent model development in [19]. EE of programming languages was studied in [26], while energy and carbon consumption testing for AI-driven Internet of Things (IoT) services were developed in [20].

*Existing Metrics and Scope Mapping to OSI and CCRA standards:* Table I summarizes the relevant existing telecommunications (columns 2 and 3), data center (columns 4-6), and deep learning (columns 7-10) metrics proposed to quantify the energy cost of data collection and manipulation. The telecommunication metrics are well established, however they measure EE and energy per bit respectively on the physical layer as summarized in the table. These EE metrics were sufficient for previous generations of mobile communication systems, but they cannot capture the AI aspects to be used for implementing 6G network functionality as well as for optimizations [15]. Furthermore, according to [27], standardization organizations have recently placed a greater emphasis on EE and energy savings as a core topic, and 3GPP, for instance, has listed EE as Key Performance Index (KPI) in its Release 19<sup>2</sup> set of specifications.

The data center consumption metrics in Table I, i.e. Power Usage Effectiveness (PUE), Carbon Usage Effectiveness (CUE), and Water Usage Effectiveness (WUE) [28], refer to the overall data center operation and include computing for AI and non AI purposes, networking and cooling. They offer a macro-system view agnostic to specifics of AI or

communications as can be seen from their description in the table (see row "description"). They implicitly quantify the energy consumption across all layers of the OSI and CCRA as shown in the rows labeled OSI Standard and CCRA Standard, but they are not designed to provide per layer analytical insights and the energy per amount of processed information.

The Deep Learning (DL) metrics summarized in columns 7-10, namely Accuracy Per Consumption (APC), Accuracy Per Energy Cost (APEC) for inference, Time To Closest APC (TTCAPC) and Time To Closest APEC (TTCAPEC) [29], consider not only the accuracy and speed of DL models but also their energy consumption and cost for training. Nevertheless, while powerful in terms of assessing the energy/performance trade-offs of models, these metrics are less suitable in assessing the energy costs of adding intelligence to future communication networks, especially in cases when the dominant energy consumption arises from data collection rather than from the model training/inference. As marked in the table (OSI Standard and CCRA Standard), their scope falls under the application layer in OSI and service layer in CCRA.

*Summary:* Inspired by the simplicity and effectiveness of metrics such as transmission efficiency through energy-per-bit and the lifecycle emissions, and responding to calls for new metrics [14], [15] that capture the energy cost in the era of AI enabled systems, this work proposes the novel Energy Cost of AI Lifecycle (eCAL) metric and methodology to derive it. eCAL is the only metric that, based on OSI and CCRA, provides insights into the cost of inference, considering the data transmission and AI model overheads.

<sup>2</sup><https://www.3gpp.org/specifications-technologies/releases/release-19>

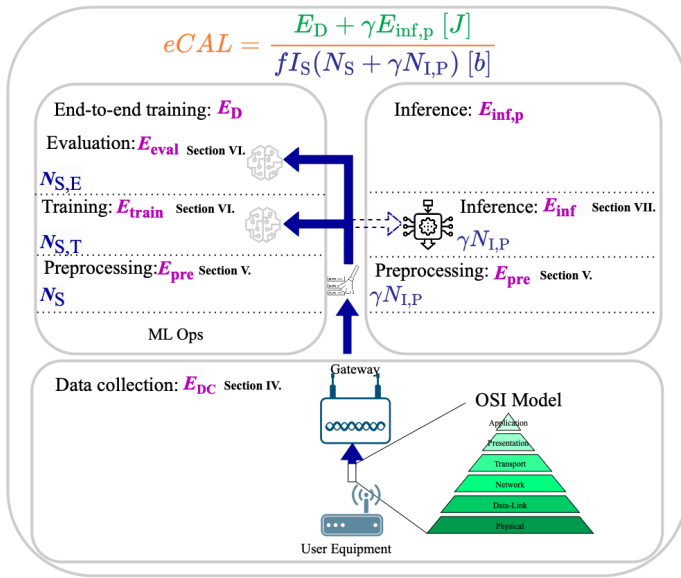


Fig. 1: Data manipulation components involved in the lifecycle of an AI model.

### III. DEFINITION AND METHODOLOGY

In our work, we consider a communication and computing system that enables the development of an AI model, whose *lifecycle* is depicted in Fig. 1, consisting of the following data manipulating components as per OSI and MLOps:

a) *Data Collection*: This data-manipulating component, depicted in the lower part of Fig. 1, represents receiving  $N_S$  data samples with  $I_S$  sample size from distributed devices via  $N_L$  independent wired or wireless links at the target computing infrastructure. The collected information can be turned into indicators such as signal strength and be interpreted by the AI models, for example, to predict the location of a user. To successfully collect all the application-level data, the total energy of data collection  $E_{DC}$  [J] is needed. The number, topology or other particularities of the data collection component of the AI model lifecycle can be adapted to specific configurations if needed.

b) *Data Preprocessing*: To ensure accuracy and reliability during the training process, the data must go through several preprocessing steps, such as cleaning, feature engineering and transformation. The energy consumption for preprocessing,  $E_{pre}$ , depends on the integrity of the ingested dataset. The proposed metric is conceptually capable of supporting also distributed or hybrid pre-processing as well as training and evaluation scenarios.

c) *Training and Evaluation*: The training component comprises the AI/ML model development using selected AI/ML techniques, such as neural network architectures, and the training data. In this step of the model development process, the processed data,  $N_{S,T}$  is fetched and utilized to learn weights and biases in order to approximate the underlying distribution. For most neural network architectures, the learning processes rely on Graphics Processing Units (GPUs)

and Tensor Processing Units (TPUs), which perform complex tensor processing operations and consume training energy,  $E_{train}$ . Once the neural network architecture weights are learned using the data in view of minimizing a loss function, the model is considered ready for evaluation and deployment. Subsequently, the quality of the learned model is evaluated on the evaluation dataset,  $N_{S,E}$ , in a process that consumes  $E_{eval}$  energy. The data storage, preprocessing, training, and evaluation form the end-to-end training of the AI/ML model and cumulatively require  $E_D$  energy to complete.

d) *Inference*: Once the model is trained and evaluated, it can be used by applications or within network scheduling and optimization components in inference mode.  $N_{I,P}$  samples of data can be sent to the AI model running in inference mode and model outputs are returned as responses in the form of forecasts for regression problems, or discrete (categorical) labels for classification problems. The energy consumption  $E_{inf}$  of a single inference is relatively small; however, for high volumes of requests, it can become significant.

#### A. Existing Metric Relevance for the Data Manipulating Components of the AI Lifecycle

Existing energy metrics offer only partial visibility into the energy demands of AI models across their full lifecycle, as illustrated in Table I. On the one hand, telecommunication and data center metrics (columns 2–6) primarily address the data collection stage. Telecommunication metrics focus on physical-layer energy consumption in the access network, while data center metrics capture aggregate energy use from all IT infrastructure. However, these metrics lack formal attribution to specific network segments or OSI layers, limiting their granularity and diagnostic utility. On the other hand, the next four columns (columns 7–10) show that existing deep learning metrics provide only coarse coverage of energy consumption during data preprocessing, training, evaluation, and inference. These metrics are typically limited to classification tasks and often rely on weight counts as proxies for energy use. Importantly, only two of them explicitly consider inference, underscoring a significant gap in coverage. Therefore, there is a need for the development and adoption of the proposed eCAL metric (column 11) as a unified, lifecycle-aware measure that enables consistent and component-resolved evaluation of energy efficiency in AI systems.

#### B. Proposed Metric

Based on the AI model lifecycle illustrated in Figure 1 and discussed in this section, we propose eCAL as *the ratio of total energy consumed by data manipulation components to the total manipulated application-level bits*:

$$eCAL = \frac{\text{Total energy of data manipulation components [J]}}{\text{Total manipulated application level data [b]}}. \quad (1)$$

eCAL introduces a fundamentally new way of looking and assessing the cost of using AI - it essentially enables to quantify the energy cost of each bit that comes out from the

TABLE II: Summary of Notations

Symbol	Description
<b>Counts</b>	
$N_S$	No. of collected data samples
$N_L$	No. of independent links
$N_{dev,cycle}$	No. of processing cycles per bit (device)
$N_{gateway,cycle}$	No. of processing cycles per bit (gateway)
$N_{S,T}$	No. of samples used for training
$N_{S,E}$	No. of samples used for evaluation
$N_{S,inf}$	No. of samples used for inference
$N_{epochs}$	No. of training epochs
$N_{batch}$	No. of batches during training
$I_S$	Sample size
$\gamma$	No. of inferences over model lifecycle
$B_T$	No. of transmitting bits
$B_{T,LOSI}$	No. of requested bits by the application from the device
$B_{T,l}$	No. of bits need to be processed at the $l$ -th layer
$M_l$	No. of nodes in the $l$ -th layer
$L_{OSI}$	No. of OSI layers
$L$	No. of dense layers
$C_{in}$	No. of input channels
$G$	No. of intervals in the grid
$N_f$	No. of filters
$N_{head}$	No. of heads
$N_{decoder,blocks}$	No. of decoder blocks
$N_{I,P}$	No. of samples used for inference
<b>Computational Complexity (CC)</b>	
$M_C$	CC of decryption
$M_{DS}^{min,max}$	CC of min-max scaling
$M_{DS}^{norm}$	CC of normalization
$M_{DS}^{GADF}$	CC of GADF
$M_{pre}$	CC of preprocessing
$M_{MLP}$	CC of a MLP
$M_{MLP,FP}$	CC of a forward propagation of MLP
$M_{CONV}$	CC of a convolutional layer
$M_{POOL}$	CC of a pooling layer
$M_{CNN,FP}$	CC of a forward propagation of CNN
$M_{KAN}$	CC of a KAN layer
$M_{NLF}$	CC of B-spline activation function across all input elements
$M_{KAN,FP}$	CC of a forward propagation of KAN
$M_{ATT}$	CC of an attention block
$M_{TR}$	CC of the decoder in a transformer
$M_{TR,FP}$	CC of a forward propagation of a transformer
$M_{model,tot}$	CC of training a model
<b>Power</b>	
$P_T$	Transmitting power
$P_R$	Receiving power
$P_{dev,cycle}$	Power consumption per processing cycle (device)
$P_{Gateway,cycle}$	Power consumption per processing cycle (Gateway)
$P_{pre}$	Power consumption of the preprocessing unit
<b>Energy Consumption (EC)</b>	
$E_T$	EC of transmitting data from device to the reception side
$E_R$	EC of receiving the signal at the reception side
$E_C$	EC of decryption
$E_{R,tot}$	EC of receiving the signal and decryption
$E_{DC}$	EC of the data collection component
$E_{DC,b}$	EC per bit of the data collection component
$E_{pre}$	EC of preprocessing
$E_{train}$	EC of model training
$E_{eval}$	EC of model evaluation
$E_{inf}$	EC of inference
$E_D$	EC of developing the model
$E_{D,b}$	EC per bit of developing the model
$E_{inf,p}$	EC of the inference process
$E_{inf,p,b}$	EC per bit of the inference process
$eCAL_{abs}$	EC over the lifetime of an AI model in the system
$eCAL$	EC per bit over the lifetime of an AI model in the system
<b>Time</b>	
$T_T$	Transmitting Time
$T_{pre}$	Executing time for preprocessing
<b>Parameters</b>	
$f$	Bit precision
$\gamma_l$	Scaling factor between DP and CP overheads
$\gamma_v$	Scaling factor for virtualization
$\beta$	Split ratio between training and evaluating data
$OH_{dp,l}$	DP overhead of the $l$ -th OSI layer
$OH_{cp,l}$	CP overhead of the $l$ -th OSI layer
$RR_{dp,l}$	DP retransmission rate of the $l$ -th OSI layer
$RR_{cp,l}$	CP retransmission rate of the $l$ -th OSI layer
$R_T$	Transmitting rate
$R_R$	Receiving rate
$B$	Batch size
$PU_{performance}$	Theoretical peak performance of a processing unit
$M_{PU}$	Computational power of a processor
$I_r$	Input tensor size (height)
$I_c$	Input tensor size (width)
$K_r$	Kernel (filter) height
$K_c$	Kernel (filter) width
$P_r$	Padding size (height)
$P_c$	Padding size (width)
$S_r$	Stride value (height)
$S_c$	Stride value (width)
$K$	Spline order
$C$	Context length
$N_{embed}$	Size of the embedding
FFS	Feed forward size

inference of an AI model over its entire lifetime while accounting for the underlying overheads. The purpose of eCAL is to measure the overall energy consumption of any AI model developed using data and a neural network architecture, independent of the use case and accuracy/performance expected by that use case, similarly as for instance, EE from Table I is applicable to various communication modules independent on their spectral efficiency. As illustrated in Table I, eCAL is the only metric able to capture the energy costs in communication networks following the standard OSI model by modeling the overheads introduced by various layers as well as two of the layers of the standard CCRA in cloud computing. All the other metrics have a narrower scope and do not center on and include the actual AI training and inference. In future when a metric such as eCAL may be standardized, it could be used as an energy badge on any AI model, in a similar fashion as there are CO<sub>2</sub> footprint badges used when booking flights or EE classes used on household appliances.

### C. Methodology

In the upcoming sections, we derive the proposed metric for example case studies that comply with the OSI standard architecture and MLOps framework that is part of the platform layer in the CCRA standard architecture. We follow the data flow, highlighted with blue in Fig. 1, across the above-mentioned components and derive the computational complexity and subsequently the energy consumption, highlighted with purple, in each component. In Section IV, we derive  $E_T$  for the data collection component. With this formalism in place, Section VIII is concerned with deriving eCAL under specific configuration assumptions, without limiting the scope of the proposed metric. For the sake of clarity and convenience, we summarize the notations used throughout this paper in Table II.

## IV. ENERGY COST OF DATA COLLECTION

In this section, we derive the energy cost of *data collection* in an AI-powered wireless system. To calculate this cost, we first determine the number of bits that need to be transmitted from a device to the server via wireless technology (uplink). Then, we calculate the energy consumption of transmitting and receiving the data, based on the given transmission and reception power and the corresponding data rate. Finally, we derive the total energy consumption for collecting data from a device. The assumption is that all data is collected via a single link; however, a summation can be added to generalize data collection to multiple links with different parameters. In this regard, the modular and extensible open source calculator can be extended to include specific communication segments, topologies, and technologies employing various resource allocation and optimization techniques.

### A. OSI Overhead Estimation Method in eCAL

In OSI architecture, each layer introduces its own overhead, including various header fields in the Data Plane (DP) and additional control and set-up messaging from the Control Plane (CP). Additionally, in some of the layers, such as link (e.g.,

MAC) and transport (e.g., TCP) layers, errors or packet loss are internally treated, potentially leading to retransmissions. While each protocol and every layer enables a wide selection of settings, we devise the following generalized theoretical formulation for computing the size of the transmitted data at the physical layer ( $B_T$ ):

$$B_T [b] = \lceil B_{T,LOSI} \prod_{l=1}^{LOSI} \underbrace{(RR_{DP,l}(1 + OH_{DP,l}))}_{\text{contribution from DP}} + \underbrace{RR_{CP,l}\gamma_l OH_{CP,l}}_{\text{contribution from CP}} \rceil, \text{ where } LOSI = 7, \quad (2)$$

where  $B_{T,LOSI}$  represents the application layer data (e.g. telemetry) sent from the device, measured in bits. It is calculated as the product of the bit precision ( $f$ ), the number of *samples* ( $N_S$ ) and the *sample size* ( $I_S$ ) in floating-point format, i.e.,  $B_{T,LOSI} = fN_S I_S$ . Typically,  $f$  equals 32 bits for single precision (float) or 64 bits for double precision format. To be able to send/receive data, in each of the seven OSI layers, represented by the product in Eq. (2), a number of data and control plane operations take place as expressed in the respective terms. The application data,  $B_{T,LOSI}$ , is processed and is added some overhead  $OH_{DP,l}$ , in some layers it is encrypted (i.e. application, presentation and/or transport layers) and in some layers it may also require retransmissions  $RR_{DP,l}$ . Moreover, some layers, such as the network layer, incur additional overhead required from signaling to maintain routing tables. This is reflected in the second term of Eq. (2) through the respective CP overheads  $OH_{CP,l}$ , retransmissions  $RR_{CP,l}$  and the  $\gamma_l$  scaling factor that adjusts for the relative contribution of the CP overhead compared to the DP counterpart at the  $l$ -th layer. The scaling factor can also be used to compensate for other specific overheads unforeseen by the considered configuration in this paper, such as the fiber-based wired communication backhaul.

*Numerical Validation:* The eCAL calculator implements the computation from Eq. (2) and enables the configuration of the application data size, retransmission rates, overheads, and scaling factor. Furthermore, it enables plugging custom protocol implementations for each of the layers, based also on the existing literature [30]–[32], so that the community can also instantiate eCAL for a specific well-defined set of protocols in addition to the approach adopted in this paper.

To illustrate the behavior of Eq. (2), we first consider a scenario where a single device transmits  $N_S$  of double-precision samples to the application accompanied by DP and CP overheads while altering the retransmission rate. In particular, we consider that each layer in the OSI model introduces a fixed overhead percentage for the DP and CP, with 10% and 5%, respectively. Furthermore, the relative contribution of CP overhead is scaled by a factor of 0.5, i.e.,  $\gamma_l = 0.5$ . The retransmission rates for both DP and CP are assumed to be equal and vary from 1 to 2 in increments of 0.04. This is shown in Fig. 2. The results show the retransmission rate has a significant impact on total transmitting bits. For example, when  $N_S = 256$  samples, there is a growth of 2.3, 17, and

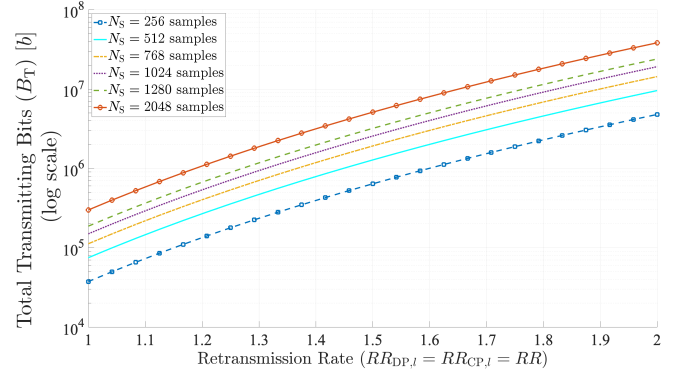


Fig. 2: Total transmitting bits ( $B_T$ ) versus retransmission rate with  $\gamma_l = 0.5$ ,  $OH_{DP,l} = 10\%$  and  $OH_{CP,l} = 5\%$ .

128 times with retransmission rates equal to 1.125, 1.5, and 2, respectively, compared to scenarios with no retransmission.

### B. Application Layer Centered Energy Estimation for the Data Collection Component of eCAL

To estimate the energy consumption of the data collection component ( $E_{DC}$ ), which is the sum of the energy of transmitting ( $E_T$ ) and receiving the data ( $E_R$ ) introduced in the physical layer (PHY), as well as the energy consumption of computation in the DP and CP across the various layers of OSI ( $E_C$ ). We consider a network comprising  $N_L$  independent and direct links between nodes, which covers all the network topologies, including multi-access and multi-hop links. We propose the following analytical expression for the  $p$ -th links, which includes:

$$E_{DC,p} = \underbrace{\frac{P_{T,p}[W]}{R_{T,p}[b/s]} B_{T,p}[b]}_{\text{PHY layer transmitting energy } (E_{T,p})} + \underbrace{\frac{P_{R,p}[W]}{R_{R,p}[b/s]} B_{T,p}[b]}_{\text{PHY layer receiving energy } (E_{R,p})} + \sum_{l=2}^{LOSI} \underbrace{(B_{T,l,p} [b] N_{\text{dev,cycle},l,p} [c/b] P_{\text{dev,cycle},p} [J/c])}_{\text{from MAC to APP layer computational energy at the device}} + \underbrace{B_{T,l,p} [b] N_{\text{gateway,cycle},l,p} [c/b] P_{\text{gateway,cycle},p} [J/c]}_{\text{from MAC to APP layer computational energy at the gateway}}, \quad (3)$$

where  $P_{T,p}$  and  $R_{T,p}$  represent the transmitting power and the data rate, respectively, while  $P_{R,p}$  and  $R_{R,p}$  are the receiving power and data rate. Furthermore,  $B_{T,l}$  denotes the total number of bits that need to be processed at the  $l$ -th layer in the OSI model. Additionally, we define the computational parameters at the device as  $N_{\text{dev,cycle},l,p}$  representing the number of processing cycles per bit at the  $l$ -th layer, and  $P_{\text{dev,cycle},p}$ , denoting the power consumption per cycle. Similarly, at the gateway, these parameters are defined as  $N_{\text{gateway,cycle},l}$  and  $P_{\text{gateway,cycle},p}$ . As a result, we can calculate the total energy cost of the data collection as the sum of all  $N_L$  links, which is expressed as:

$$E_{DC} = \sum_{p=1}^{N_L} E_{DC,p}. \quad (4)$$

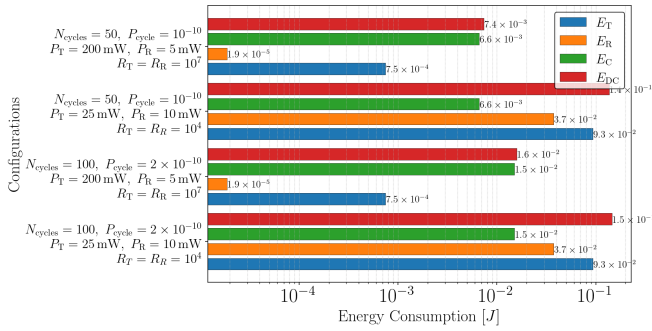


Fig. 3: Energy consumption of data collection ( $E_{DC}$ ) (log scale) with its components and configurations, including transmission energy ( $E_T$ ), receiving energy ( $E_R$ ), and computational energy ( $E_C$ ) with  $N_S = 256$ ,  $RR_{DP,l} = RR_{CP,l} = 1$ ,  $OH_{DP,l} = 10\%$ ,  $OH_{CP,l} = 5\%$ , and  $\gamma_l = 0.5$ .

*Numerical Validation:* Computing exact values for  $E_{DC}$  for a broad range of  $B_{T_l}$ ,  $N_{\text{cycle},l}$ , and  $P_{\text{cycle}}$  is challenging due to the overall complexity of computing systems. For instance,  $N_{\text{cycle},l}$  varies across microprocessors when processing the same amount of data, and it does not have a linear dependency with data size [33]. Therefore, the values for  $B_{T_l}$  and  $N_{\text{cycle}}$  cannot be chosen arbitrarily. Next,  $P_{\text{cycle}}$  also depends on the microprocessor. However, in Fig. 3, we illustrate the energy consumption of  $E_{DC}$  with a selected set of values to provide an intuition on the contribution from each term. More specifically, we analyze a scenario where  $N_S = 256$ , and we consider two sets of parameters to compute transmitting and receiving energy, i.e.  $E_T$  and  $E_R$ , alongside two different settings for calculating the computational energy consumption ( $E_C$ ). The results show that while transmission energy ( $E_T$ ) remains the dominant contributor in most cases, the computational energy consumption ( $E_C$ ) is not negligible and, in some configurations, constitutes a significant portion of the total energy consumption of data collection. This is particularly the case when the hardware is less optimized for the tasks [33], leading to higher cycles per bit ( $N_{\text{cycle},l}$ ) and power per cycle ( $P_{\text{cycle}}$ ). For example, when  $N_{\text{cycle}} = 100$  and  $P_{\text{cycle}} = 2 \times 10^{-10}$ ,  $E_C$  is  $1.51 \times 10^{-2}$  [J], which represents approximately 10% and 95% of the total energy cost in two different PHY configurations. On the other hand, when  $N_{\text{cycle},l} = 50$  and  $P_{\text{cycle}} = 10^{-10}$ ,  $E_C$  is  $6.61 \times 10^{-3}$  [J], contributing to approximately 5% and 90% of the total energy consumption in data collection component.

TABLE III: Comparison of EE when transmitting 0.1 Mbits

Tech	EE w/ $E_{DC}$ (Mbit/J)	EE (Mbit/J)
Wi-Fi (8 UEs)	17.07	17.42
Wi-Fi (1 UE)	41.31	41.32
5G	1.63	1.65

*Empirical Validation:* To further validate our approach in a real-world setting, empirical measurements from Wi-Fi and 5G networks are considered. Specifically, in [34], the authors

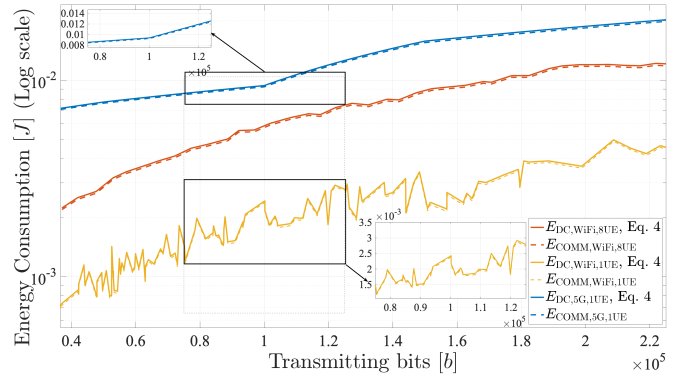


Fig. 4: Proposed  $E_{DC}$  comparison with real-world measurement data.

conducted rigorous measurements of various parameters, such as orthogonal frequency-division multiple access (OFDMA) throughput, latency, and power consumption achieved by Wi-Fi 6 technology, i.e., IEEE 802.11ax, using commercial devices. For 5G measurements, we consider the experiment conducted in [35], where a mobile user equipment (UE) is connected to a commercial 5G modem.

The results are shown in Fig. 4. The proposed  $E_{DC}$  consistently serves as a tight upper bound across both technologies, and hence corresponds to a lower bound on achievable EE (bits per Joule). For example, under the same bit window size of  $0.75$  to  $1.2 \times 10^5$  [b] the measured energy consumption ( $E_{COMM,\cdot}$ ) of 5G (highlighted in blue), Wi-Fi 6 in a multi-access scenario (8 UEs, highlighted in red), and single UE (highlighted in orange) are  $8.4$  to  $12.4$  [mJ],  $4.1$  to  $7.2$  [mJ], and  $1.4$  to  $2.75$  [mJ], respectively. The proposed approach to the corresponding cases are  $9.38$  to  $15.8$  [mJ],  $6.03$  to  $8.63$  [mJ],  $1.82$  to  $3.41$  [mJ]. Moreover, the comparison of the EE when transmitting 0.1 Mbits of data can be seen in Table III. As discussed, the proposed approach serves as a tight lower bound for EE. In other words, if we put the energy consumption of the computational part into consideration, this data-manipulating component will be less energy efficient than only considering physical layer measurement.

The methodology used for obtaining these results is as follows. We aggregate and process three datasets that are collected in real-world measurements, corresponding to uplink with 8 UEs (1 mobile UE and 7 Personal Computers (PCs) with Wi-Fi), uplink with a single mobile UE (Wi-Fi), and single UE in a commercial 5G network. For the Wi-Fi scenarios, we extract device-side transmission energy and device specifications from measurements to parameterize the UE terms in Eq. (3); for the access point (AP) (ASUS RT-AX58U), we use hardware specifications to obtain the receiving and computing terms in Eq. (3). To model the OSI-stack overhead, we use published cryptography and networking guidance. On mobile UE (Galaxy S10, ARMv8 with cryptography extensions) [36], we assign  $0.3$  [c/b] from transport to application layer (L4 to L7) and  $0.1$  [c/b] at the medium access control (MAC) and Network layer (L2 and L3). These numbers are consistent

with Advanced Encryption Standard (AES)-based encryption throughput on ARM-based architectures with hardware acceleration reported in OpenSSL microbenchmarks [37]. On PCs (Intel AX210 NICs) and AP, link-layer security and MAC functions are Network Interface Card (NIC)-offloaded. Therefore, we assume 0.02 [c/b] (application), 0.01 [c/b] (TCP/IP protocol), and 0.005 [c/b] (MAC), aligned with Intel AES documentation and NIC offload literature [38], [39]. Guided by [40], we set 0.3 [nJ/c] and 0.1 [nJ/c] on ARM and Intel-based systems, respectively. For 5G measurement, we can obtain the receiving power and the receiving data size. It is mentioned in [41] that the pathloss follows the 3GPP UMa model, so we can then obtain the transmitting power. To account for protocol stack overhead, we set the overhead for L2 to L6 as 0.2 and L7 as 0.1. Since the setup of UE and AP is similar to the Wi-Fi scenario (same UE and Intel-based processor), the computing parameters are assumed to be the same as in the Wi-Fi scenario. These parameters help to anchor the derived  $E_{DC}$  to realistic hardware capabilities at practical operating points.

## V. ENERGY COST OF DATA PREPROCESSING

At the server side, data is first stored on a hard drive, subsequently preprocessed, and finally used for the ML model development or inference. This section focuses on preprocessing, while inference is addressed in Section VII.

Storage is generally energy-efficient, with relatively negligible energy costs. However, it can become significant when handling large volumes of incoming data or when utilizing virtualized hosted storage with encryption in an edge-cloud environment [42]. In the following case study, we consider the dataset with  $N_S$  samples collected via the wireless network, as depicted in Fig. 1 and discussed in Section IV. We also consider data preprocessing consisting of *data cleaning*, and *data transformation* steps, while leaving other more complex approaches, such as feature engineering, for further extensions of the study and simulation tool.

In the *data cleaning* step, the task of preprocessing is to identify and remove invalid samples from a list or array, which incurs zero floating-point operations (FLOPs)<sup>3</sup>, as no floating-point additions or multiplications are performed, only comparisons and memory operations. During the *data transformation* step, preprocessing involves determining the complexity of data transformation ( $M_{DS}$ ). We provide three examples, i.e., min-max scaling, normalization, and Gramian Angular Difference Field (GADF) process, which represent typical approaches for data transformation.

*a) Min-max scaling:* Min-max scaling is a data preprocessing technique that transforms numerical data to fit within the [0,1] interval by scaling each value relative to the minimum and maximum values in the dataset. For each feature, the transformation subtracts the minimum value and divides by the range, ensuring that the lowest value becomes 0 and

<sup>3</sup>FLOPs are often used to enable theoretical estimation of computational complexity. Alternative approaches would involve direct energy measurements through interfaces such as PAPI or tools such as Scaphandre.

the highest value becomes 1, with all other values scaled proportionally between them. While finding the minimum and maximum values requires computational resources for comparisons, these operations do not contribute to the FLOPs count. The scaling itself requires calculating the range (one FLOP), followed by subtracting the minimum and dividing by the range for each sample ( $2N_S I_S$  FLOPs). Therefore, the total number of FLOPs ( $M_{DS}^{\min\max}$ ) for min-max scaling can be expressed as:

$$M_{DS}^{\min\max} = 2N_S I_S + 1. \quad (5)$$

*b) Normalization:* Standard score, also known as z-score normalization, represents a more computationally intensive preprocessing technique that involves three distinct computational steps. First, calculating the population mean requires  $N_S I_S$  FLOPs, as we sum all values and divide by the total number of samples. Second, computing the population standard deviation demands  $3N_S I_S + 1$  FLOPs, which encompasses calculating squared differences from the mean, their sum, and the final square root operation. Finally, the standardization transformation necessitates  $2N_S I_S$  FLOPs, as each data point must be centered by subtracting the mean and divided by the standard deviation for scaling. The total computational cost for normalization, expressed in FLOPs ( $M_{DS}^{\text{norm}}$ ), is therefore:

$$M_{DS}^{\text{norm}} = 6N_S I_S + 1. \quad (6)$$

*c) Gramian Angular Difference Field:* To showcase an even more computationally expensive preprocessing operation, we implemented a calculator to compute the energy cost of the GADF transformation [43]. This transformation converts time series data into an image representation that captures temporal correlations between each pair of values in the time series. The GADF computation consists of several sequential steps, each contributing to the overall computational complexity and, consequently, the energy consumption. The first step requires scaling the time series data using min-max scaling, which ensures that values fall within the [-1, 1] interval. Following the scaling, the data undergoes conversion to polar coordinates, where the radius is calculated using the time stamp values, and the angular coordinates are computed through an inverse cosine operation. The final step involves constructing the GADF matrix through pairwise angle differences, resulting in an  $I_S \times I_S$  matrix where  $I_S$  represents the length of the input time series.

The computational complexity of GADF can be broken down into its constituent operations. The initial min-max scaling requires  $2N_S I_S + 1$  FLOPs as previously discussed. However, in this case we have to multiply the number of samples with the length of the input time series ( $I_S$ ) as we are dealing with a series of values in a single sample increasing the FLOPs. The polar coordinate transformation and the construction of the GADF matrix requires  $(5I_S + I_S^2)N_S$  FLOPs. Therefore, the total number of FLOPs ( $M_{DS}^{\text{GADF}}$ ) for the GADF transformation can be expressed as:

$$M_{DS}^{\text{GADF}} = (2N_S I_S + 1) + (5I_S + I_S^2)N_S. \quad (7)$$

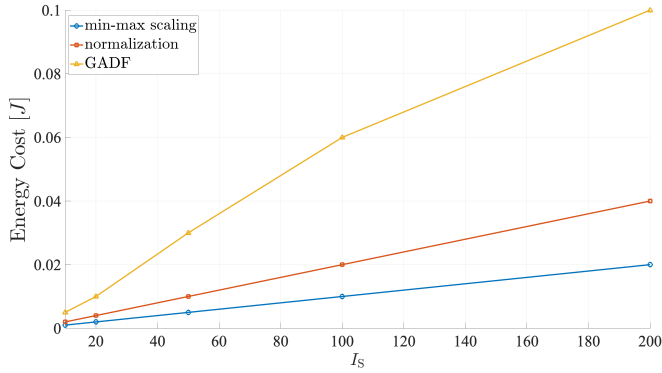


Fig. 5: Energy consumption ( $E_{\text{pre}}$ ) of different sample size ( $I_S$ ) across different preprocessing techniques.

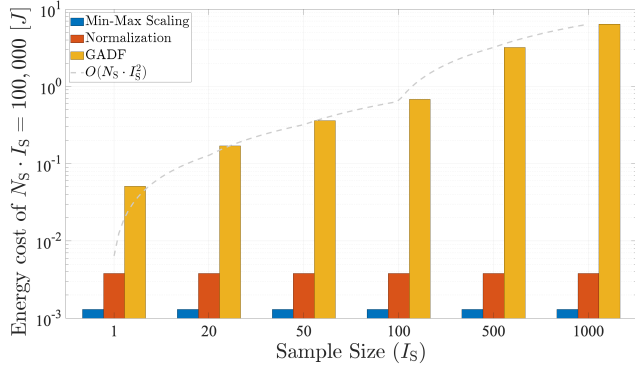


Fig. 6: Energy consumption ( $E_{\text{pre}}$ ) of fixed data point ( $N_S I_S$ ) across different preprocessing techniques and sample size ( $I_S$ ).

This quadratic computational complexity makes GADF significantly more energy-intensive compared to simpler preprocessing operations like standardization or min-max scaling, particularly for longer time series. As a result, the total number of FLOPs for preprocessing can be expressed as:

$$M_{\text{pre}} = \begin{cases} 2N_S I_S + 1, & \text{min-max scaling,} \\ 6N_S I_S + 1, & \text{normalization,} \\ 2N_S I_S + 1 + (5I_S + I_S^2)N_S, & \text{GADF.} \end{cases} \quad (8)$$

With the computing complexity in FLOPs formalized, we can obtain total energy consumption ( $E_{\text{pre}}$ ) of the preprocessing ( $E_{\text{pre}}$ ) by utilizing the power consumption of the processing unit ( $P_{\text{pre}}$ ) and the executing time ( $T_{\text{pre}}$ ):

$$E_{\text{pre}}[\text{J}] = P_{\text{pre}}[\text{W}]T_{\text{pre}}[\text{s}], \quad (9)$$

where  $T_{\text{pre}}$  can be calculated as the ratio between FLOPs needed for preprocessing and the computational power of a processor ( $M_{\text{PU}}$ ):

$$T_{\text{pre}}[\text{s}] = \frac{M_{\text{pre}}[\text{FLOPs}]}{M_{\text{PU}}[\text{FLOPs/s}]}. \quad (10)$$

*Numerical Validation:* To illustrate the energy cost in various  $N_S$  and  $I_S$  configurations, consider the preprocessing energy cost  $E_{\text{pre}}$  on a CPU with  $M_{\text{PU}} = 10$  GFLOPs/s and power consumption of  $P_{\text{pre}} = 140$  W, shown in Fig. 5

and Fig. 6. More specifically, Fig. 5 demonstrates how the energy consumption of preprocessing methods for a fixed number of samples ( $N_S = 256$ ) increases with the sample size ( $I_S$ ). This trend is consistent across min-max scaling, normalization, and GADF, with GADF exhibiting the most pronounced energy growth due to its quadratic dependency on  $I_S$ , whereas, the energy cost of the other two techniques grows linearly. In addition, Fig. 6 focuses on the energy consumption of the preprocessing techniques while maintaining a constant total amount of data ( $N_S I_S = 100,000$ ). This constraint ensures that as the sample size ( $I_S$ ) increases, the number of data samples ( $N_S$ ) decreases proportionally. Consequently, the energy consumption for min-max scaling and normalization remains constant across different configurations, as their computational complexity scales linearly with  $N_S I_S$ . In contrast, GADF exhibits a quadratic (with a linear component) growth in energy consumption due to the  $I_S^2$  term in its computational complexity, shown in Eq. (8), which is also confirmed by the  $O(N_S I_S^2)$  shown in the gray dotted line. These results highlight the trade-offs in selecting a preprocessing method based on both the EE requirements and the specific input data characteristics required by the AI/ML technique.

## VI. ENERGY COST OF TRAINING

To train a model, training data and machine learning techniques are needed. In this study, we consider neural network architectures with centralized offline training, however, extensions of this work could consider online, distributed, federated or transfer approaches as well. As discussed in Section V, the training data typically goes through a preprocessing phase and is then split into training and evaluation sets, with a  $\beta$  split ratio as:

$$N_S = \underbrace{\beta N_S}_{N_{S,T}} + \underbrace{(1-\beta)N_S}_{N_{S,E}}, \quad (11)$$

where  $N_{S,T}$  and  $N_{S,E}$  represent the number of samples for training and evaluation, respectively. For studying the energy cost of training, in this paper we focus on four representative neural network architectures<sup>4</sup>, namely, Multilayer Perceptrons (MLPs) [11], Convolutional Neural Networks (CNNs) [44], Kolmogorov–Arnold Networks (KANs) [45], and transformers [46]. MLPs established the foundations of deep learning as universal function approximators, enabling the first wave of practical neural network models. CNNs marked a breakthrough by exploiting spatial hierarchies, revolutionizing computer vision and inspiring domain-specific architectures. Transformers represent the most recent paradigm shift, introducing attention mechanisms that now dominate language processing through the GPT models. Finally, KANs are included as a novel, explainable architecture compared to MLPs.

Training a neural network involves two fundamental phases: *forward propagation* and *backward propagation*, depicted with blue and red arrows in Fig. 7, respectively, on an example MLP. During the forward propagation, input data passes

<sup>4</sup>Note that the implementation of the calculator supports many other architectures using pytorch.

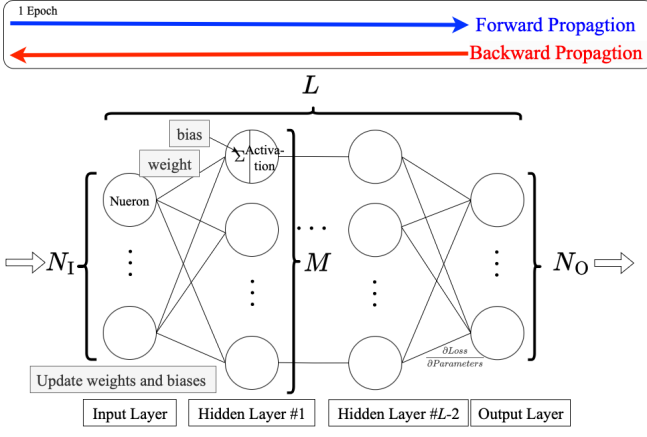


Fig. 7: A fully connected MLP architecture.

through the network layers. Each layer performs specific tasks, such as computing a linear combination of weights and biases, followed by applying activation functions in dense (fully connected) layers. Convolutional layers perform convolutional operations, while pooling mechanisms are applied on pooling layers. At the end of this phase, the loss is calculated by comparing the predicted outputs to the actual target values. Subsequently, the model performs backward propagation, where it calculates gradients of the loss with respect to each parameter, updates these gradients in reverse order through the layers, and adjusts the weights and biases accordingly. This process completes one epoch. Consequently, we can calculate the energy costs associated with forward and backward propagation, leading to an understanding of the overall energy consumption for training, model evaluation, and subsequent inference. In the following subsections, we showcase the computational complexity of training and evaluating the aforementioned Neural Networks (NNs).

#### A. Computational Complexity of MLP, CNN, KAN and transformer

a) *MLPs*: Assuming an MLP architecture with  $L$  dense layers as depicted in Fig. 7, where  $L = K + 2$ , the total number of FLOPs for the forward propagation of a single input sample can be expressed as:

$$M_{\text{MLP}} = \sum_{l=1}^{L-1} \left( \underbrace{(2M_{l-1}M_l)}_{\text{Weight and bias}} + \underbrace{2M_l}_{\text{Summation and activation}} \right), \quad (12)$$

where the first term in the sum represents one multiplication and one addition ( $= 2$  FLOPs) related to the weight and bias corresponding to the edges times the number of nodes in that layer ( $= M_{l-1}M_l$ ), while the second term represents the summation of all the values of the incoming edges and the application of the activation function ( $= 2$  FLOPs) times the number of nodes in that layer ( $M_l$ ).

In general, however, training consists of multiple epochs and batches. Therefore, the total complexity of forward propagation is:

$$\begin{aligned} M_{\text{MLP,FP}} &= N_{\text{epochs}} N_{\text{batch}} B M_{\text{MLP}} \\ &= N_{\text{epochs}} N_{\text{S,T}} M_{\text{MLP}}. \end{aligned} \quad (13)$$

b) *CNNs*: Typical CNNs consist of three types of layers: dense layers, convolutional layers, and pooling layers. For a convolutional layer, with input tensor of size  $I_r \times I_c \times C_{\text{in}}$ , the corresponding computational complexity is delivered as:

$$\begin{aligned} M_{\text{CONV}} &= \underbrace{\left( \frac{I_r - K_r + 2P_r}{S_r} + 1 \right)}_{\text{Output height}} \underbrace{\left( \frac{I_c - K_c + 2P_c}{S_c} + 1 \right)}_{\text{Output width}} \\ &\quad \underbrace{\left( C_{\text{in}} K_r K_c + 1 \right)}_{\text{Computation per filter}} \underbrace{N_f}_{\text{No. of filters}}, \end{aligned} \quad (14)$$

where  $K_r$  and  $K_c$  are the kernel (filter) height and width,  $P_r$  and  $P_c$  are the padding sizes for height and width,  $S_r$  and  $S_c$  are the stride values for height and width, and  $N_f$  is the number of filters in the layer. For down-sampling the input tensor data, a pooling layer is needed, and the number of FLOPs of such layer is expressed as:

$$M_{\text{POOL}} = \underbrace{\left( \frac{I_r - K_r}{S_r} + 1 \right)}_{\text{Output height}} \underbrace{\left( \frac{I_c - K_c}{S_c} + 1 \right)}_{\text{Output width}} \underbrace{C_{\text{in}}}_{\text{Input channels}}. \quad (15)$$

Thus, the total number of FLOPs for the forward propagation of a single input sample in a CNN can be calculated by summing the contributions across all layer types [47]. As a result, the total FLOPs of a CNN is:

$$\begin{aligned} M_{\text{CNN,FP}} &= N_{\text{epochs}} N_{\text{S,T}} \\ &\quad \left( \sum_{l=1}^{L_c} M_{\text{CONV}} + \sum_{l=1}^{L_p} M_{\text{POOL}} + M_{\text{MLP}} \right). \end{aligned} \quad (16)$$

c) *KANs*: KANs leverage the Kolmogorov-Arnold representation theorem to decompose complex multivariate functions into univariate sub-functions. This is achieved through the use of learnable B-spline activation functions and shortcut paths [45]. Unlike MLPs, which apply fixed activation functions to nodes, KANs feature learnable activation functions on edges, providing greater flexibility and interpretability. According to [48], the computational complexity of a single KAN layer can be computed as:

$$\begin{aligned} M_{\text{KAN}} &= \sum_{l=1}^{L-1} \left( \underbrace{M_{\text{NLF}} M_{l-1}}_{\text{From B-spline}} \right. \\ &\quad \left. + \underbrace{(M_{l-1} M_l) [9K(G + 1.5K) + 2G - 2.5K + 3]}_{\text{Input and output B-spline and grid}} \right) \\ &= \sum_{l=1}^{L-1} (M_{\text{NLF}} M_{l-1} + (M_{l-1} M_l) M_B), \end{aligned} \quad (17)$$

where  $M_{\text{NLF}}$  denote as the number of FLOPs contributed from the B-spline activation function across all input elements. The second term accounts for the computational costs arising from

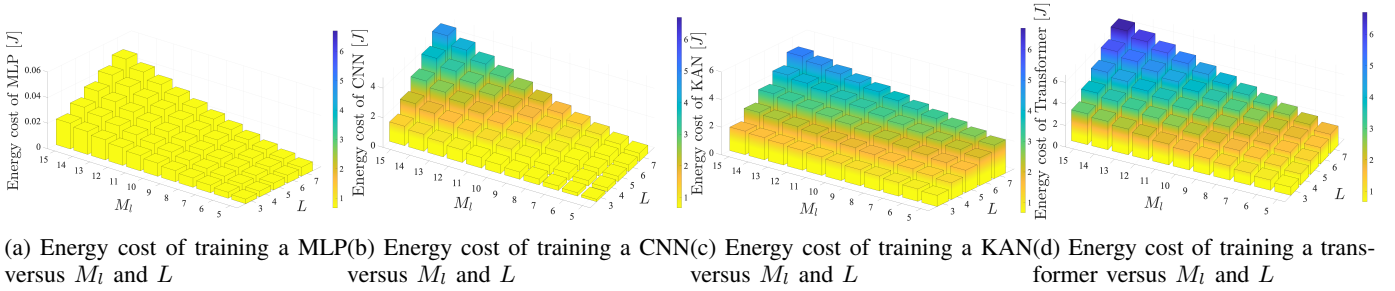


Fig. 8: Energy cost of training different models with respect to the number of nodes ( $M_l$ ) and layers ( $L$ ).

the combination of input and output dimensions ( $M_{l-1}$  and  $M_l$ ) with the operations performed by the B-spline transformation. These operations include the iterative evaluation of spline basis functions and the associated transformations, governed by the spline order ( $K$ ) and the number of intervals in the grid ( $G$ ). The total FLOPs of a KANs network is calculated as the sum of all KAN layers similarly as in the case of MLPs in Eq. (13), where total  $L$  layers can be expressed as:

$$M_{\text{KAN,FP}} = N_{\text{epochs}} N_{\text{S,T}} M_{\text{KAN}}. \quad (18)$$

*d) Transformer:* Based on the attention mechanism, the transformers [46] represent a paradigm shift in deep learning, replacing traditional architectures such as CNN with self-attention mechanisms. While enabling significant breakthroughs in AI through efficient parallel processing and robust modeling of long-range dependencies, they are relatively complex. In addition to attention layers, the transformer architecture also includes MLP, normalization, and positional encoding, making the analytic expression for the FLOP computation intractable. Following existing literature [49] and approximations<sup>5</sup>, we approach the estimation as follows:

$$M_{\text{ATT}} = 2 \left( \underbrace{C N_{\text{embed}} 3 N_{\text{embed}}}_{\text{K, Q, V positional embedding}} + \underbrace{C^2 N_{\text{embed}}}_{\text{Attention scores}} \right) + \underbrace{N_{\text{head}} C^2 N_{\text{embed}} / N_{\text{head}}}_{\text{reduce}} + \underbrace{C N_{\text{embed}} N_{\text{embed}}}_{\text{Projection}}, \quad (19)$$

where  $C$  is the context length,  $N_{\text{embed}}$  is the size of the embedding and  $N_{\text{head}}$  is the number of heads. The complexity of the decoder in a transformer is then given by:

$$M_{\text{TR}} = N_{\text{decoder\_blocks}} (M_{\text{ATT}} + \underbrace{4 C N_{\text{embed}} FFS}_{\text{MLP blocks}}), \quad (20)$$

where  $N_{\text{decoder\_blocks}}$  and  $FFS$  stand for the number of decoder blocks and the feed-forward size, respectively. The total complexity of forward propagation is:

$$M_{\text{TR,FP}} = N_{\text{epochs}} N_{\text{S,T}} M_{\text{TR}}. \quad (21)$$

For more specific cases, such as GPT-like architectures, a final dense layer is also needed. However, this work focuses on a more general formulation of transformer models.

<sup>5</sup>[https://www.gaohongnan.com/playbook/training/how\\_to\\_calculate\\_flops\\_in\\_transformer\\_based\\_models.html](https://www.gaohongnan.com/playbook/training/how_to_calculate_flops_in_transformer_based_models.html)

## B. Energy Estimation for the Model Training

To determine the computational complexity of training a model, backward propagation needs to also be considered. The standard approximation, also confirmed in [50], is that the backward propagation requires two times the floating-point operations per cycle per core (FLOPs) of the forward propagation. In particular, backward propagation requires matrix multiplications for updating the weights and propagating the gradient. Thus, we can approximate the computing complexity of training a model with Eq. 22 and obtain the energy consumption of the entire training process with E1. 23.

$$M_{\text{model,tot}} \approx 3 M_{\text{model,FP}}. \quad (22)$$

$$E_{\text{train}} = \frac{3 M_{\text{model,FP}} [\text{FLOPs}]}{PU_{\text{performance}} [\text{FLOPs/s/W}]}. \quad (23)$$

From Eqs. (13), (16), (18), (21), and (23), we can observe that the training data set size scales linearly with energy consumption of the model training, as it does not affect the cost of a single forward/backward pass. On the other hand, training the same model on a state-of-the-art GPU with a processing power of 312 [ $TFLOPs/s$ ] and power consumption of 400 [ $W$ ] is approximately 28 times more energy efficient than using a CPU, which operates at 13.824 [ $TFLOPs/s$ ] and consumes 500 [ $W$ ].

*Numerical and Empirical Validation:* Fig. 8 illustrates the relationship between the energy consumption of a model and two architectural parameters: the number of layers and the number of nodes in a layer. As the architectures of the models become deeper and wider, the computational complexity also increases, and this leads to higher energy consumption. For instance, in the case where  $M_l = 10$  and  $L = 5$ , the energy consumption of the transformer, KAN, and CNN models are approximately 173, 149, and 81 times greater than that of the MLP model. However, some architectures, such as KANs, are known to perform better with fewer layers [45], therefore it is unlikely to find a KAN with  $L > 5$ . While at a first glance, it seems that MLPs may be significantly more energy efficient than KANs, the actual difference for the same performance will be less prominent for many applications. CNNs, and especially transformers are known to be computationally demanding and subsequently exhibit high energy consumption, while at the same time larger architectures proved better performance in various application areas.

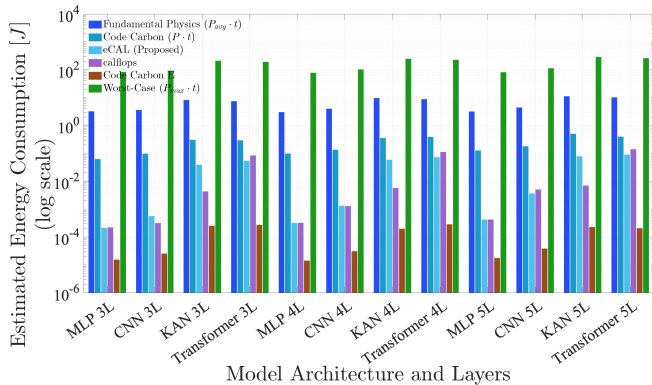


Fig. 9: Training energy consumption benchmarks for the selected fundamental neural architectures.

Fig. 9 benchmarks the model training energy required by eCAL against (a) a simple fundamental physics approach  $E = P_{avg} \cdot t$  that considers the average power consumption of the GPUs over the training time, (b) the open-source calcflops<sup>6</sup> library able to compute the theoretical amount of FLOPs for neural networks implemented in pytorch, (c) Code Carbon<sup>7</sup>, and (d) a worst case scenario that assumes the GPU is used at maximum capacity during the entire training time computed as  $E = P_{max} \cdot t$ . For eCAL as per Eq. (23), calcflops and worst case, we set the value of  $P_{max} = 10W$  as typical for an Apple M2 GPU. For the fundamental physics we measured the average power used by the GPU at  $P_{avg} = 0.38W$ <sup>8</sup> using the PowerMetrics tool. Code Carbon outputs energy, power and time duration measurements. It measures the power and time duration, plotted as Code Carbon ( $P \cdot t$ ), through system tools, such as PowerMetrics for Apple silicon or a dedicated python library for NVIDIA GPUs, while it computes the energy, plotted as Code Carbon E, based on a model. The results show that eCAL and calcflops provide very similar energy footprint estimated for MLPs, CNN and Transformers based networks. For MLPs, the difference is negligible, for CNNs eCAL slightly overestimates compared to calcflops, while for transformers it slightly underestimates. The slight differences are due to the fact that it is difficult to harmonize all hyperparameters between the theoretical expressions that reflect the neural network architectures and corresponding software implementation that instantiates pytorch models that calcflops relies on. For KANs as newer architectures, calcflops underestimates compared to the eCAL due to the fact that the implementation of the architecture relies on several optimizations that reduce the number of FLOPs compared to the theoretical expressions.

The results also show that assuming average power usage during the entire training cycle with the fundamental physics expression  $E = P_{avg} \cdot t$  overestimates the consumption. The overestimation is more prominent in simple examples

<sup>6</sup>calcflops, <https://pypi.org/project/calcflops/0.0.2/>

<sup>7</sup>Code Carbon, <https://github.com/mlco2/codecarbon>

<sup>8</sup>This study can be replicated on other set-ups with [https://github.com/sensorlab/eCAL/blob/main/scripts/All\\_Theoretical\\_Empirical\\_Training\\_Energy.py](https://github.com/sensorlab/eCAL/blob/main/scripts/All_Theoretical_Empirical_Training_Energy.py)

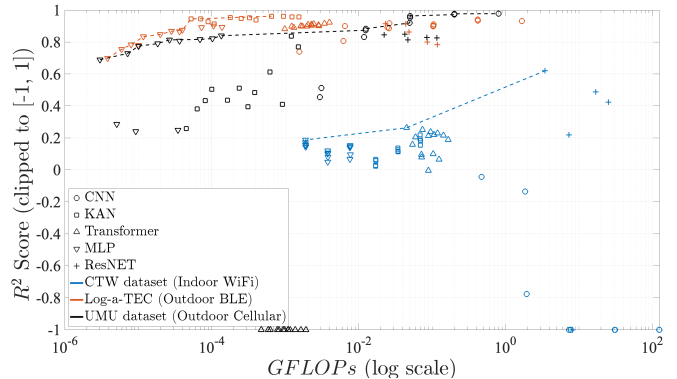


Fig. 10: Model performance (higher  $R^2$  is better) vs. computational cost (GFLOPs) for five different architectures across the three datasets. The dashed lines indicate the Pareto front.

used for this study where the data loading and model saving during training take a significant part of the training time when the GPU is not active. However, when these steps become negligible, this estimation will close in to eCAL and calcflops showing the validity of our approach. Code Carbon E measures significantly less consumed energy while Code Carbon ( $P \cdot t$ ) measures significantly more than eCAL and calcflops. These results also confirm the existing challenges regarding measuring energy and CO<sub>2</sub> footprint of software [51] and confirm the timeliness of our work.

### C. Model Evaluation

The model evaluation starts once training is complete. This functionality tests the performance of the model on a separate dataset. During the evaluation, the model processes the data using forward propagation without any adjustments to its parameters. Therefore, the energy consumption of model evaluation is expressed as:

$$E_{eval} = \frac{M_{model} N_{S,E}}{PU_{performance}}. \quad (24)$$

It is worth noting that the total energy consumption during training and evaluation is significantly influenced by the chosen evaluation strategy. While a simple train-test split requires training the model only once, more robust techniques like  $k$ -fold cross-validation necessitate  $k$  complete training cycles. For  $k$ -fold cross-validation, the total training energy consumption becomes  $k$  times the value given in Eq. (23), as the model must be retrained from scratch for each fold. Similarly, techniques such as nested cross-validation or repeated  $k$ -fold cross-validation further multiply the required training computations and corresponding energy costs, in which we have also incorporated  $k$ -fold cross-validation considerations into eCAL calculator.

To illustrate the trade-off between model performance and computational complexity, and to demonstrate how eCAL supports Pareto-front analyses, we evaluate three wireless datasets (Wi-Fi, Bluetooth Low Energy (BLE), and cellular), four fundamental architectures from Section VI, and a ResNet combining CNN and MLP blocks—a configuration known to

TABLE IV: Total energy consumption of developing ( $E_D$ ) for different models, with contributions of individual data-manipulating components.

Component	MLP	CNN	KAN	Transformer
$E_{DC}$ [J]	$8.44 \times 10^{-2}$ (89.12%)	$8.44 \times 10^{-2}$ (12.37%)	$8.44 \times 10^{-2}$ (6.31%)	$8.44 \times 10^{-2}$ (3.72%)
$E_{pre}$ [J]	$1.54 \times 10^{-6}$ (0.00%)	$1.54 \times 10^{-6}$ (0.00%)	$1.54 \times 10^{-6}$ (0.00%)	$1.54 \times 10^{-6}$ (0.00%)
$E_{train}$ [J]	$1.03 \times 10^{-2}$ (10.86%)	$5.97 \times 10^{-1}$ (87.48%)	1.25 (93.53%)	2.18 (96.12%)
$E_{eval}$ [J]	$1.72 \times 10^{-5}$ (0.02%)	$9.95 \times 10^{-4}$ (0.15%)	$2.08 \times 10^{-3}$ (0.16%)	$3.64 \times 10^{-3}$ (0.16%)
$E_D$ [J]	$9.47 \times 10^{-2}$	$6.83 \times 10^{-1}$	1.34	2.27

perform well for wireless localization [52]. Fig. 10 shows model performance ( $R^2$ ) versus computational complexity at inference time  $M_{\text{model,FP}}$ . For the univariate BLE dataset, the highest  $R^2$  scores are achieved by MLP and KAN models forming the Pareto front, while CNN, ResNet, and Transformer models underperform with higher computational costs. Similar trends appear for the 1D multivariate UMU dataset, where the Transformer performs poorly ( $R^2 = -1$ ) and is notably outperformed by simpler MLPs. With more signals (multivariate data), CNN performance improves, and these models appear on the Pareto front. On the larger, more complex multivariate CTW dataset, which includes 2D antenna array shapes, Transformer-based models perform better and also lie on the Pareto front. Overall, these results show that more complex neural architectures do not necessarily yield better performance. The balance between model complexity and accuracy depends on both the architecture and the nature and quality of the data.

## VII. ENERGY COST OF INFERENCE

The complexity of making an inference depends on the number of FLOPs required for forward propagating with input sample size  $N_{I,P}$ , i.e.,  $N_{\text{inf}} = M_{\text{model}}N_{I,P}$ . For example, when we adopt the aforementioned MLP model with  $N_{I,P} = 51$ , the complexity is calculated as  $N_{\text{inf}} = 236 \times 51 = 12,036$  FLOPs. The energy consumption of the forward propagation and the corresponding inference can be calculated as:

$$E_{\text{inf}} = \frac{M_{\text{model}}N_{I,P}}{PU_{\text{performance}}}. \quad (25)$$

We can then observe from Eqs. (24) and (25) that the cost of inference is the same as in evaluation when  $N_{S,E}$  is equal to  $N_{I,P}$ . Thus, we can conclude that the computational complexity between finishing one training and inference is on the magnitude of  $3N_{\text{epochs}}N_{S,T}/N_{I,P}$ . This indicates that the training process involves significantly more computational operations, particularly when the number of epochs or  $N_{S,T} \gg N_{I,P}$ . On the other hand, the energy consumption per bit depends on the model complexity and hardware capability. Moreover, the factor of three in the energy consumption per bit during training versus inference highlights the additional computational load inherent to training.

## VIII. eCAL: THE ENERGY COST OF AI LIFECYCLE

In this section, we describe the end-to-end energy consumption of the AI model lifecycle for making inferences with the aforementioned neural network architectures. First, we consider the energy consumption involved in developing

the model, as illustrated on the left in Fig. 1, which can be expressed as in Eq. (26) with the energy consumption per bit expressed in Eq. (27).

$$E_D = E_{DC} + E_{pre} + E_{train} + E_{eval}. \quad (26)$$

$$E_{D,b} = \frac{E_D}{fN_S I_S}. \quad (27)$$

To compare the energy consumption of all the data manipulation components required for developing and deploying an AI-enhanced system, we assume that the models are trained and evaluated using 5-fold cross-validation (as discussed in Section VI). The models require 256 samples with an input size of 10, i.e.,  $N_S I_S = 2560$ , collected from a device over a wireless network configured with the following parameters:  $P_T = 200$  [mW],  $P_R = 5$  [mW],  $R_T = R_R = 10$  [Mbps],  $N_{\text{cycle},l} = 100$  [c/b], and  $P_{\text{cycle}} = 10^{-10}$  [W/c]. We also assume the link between the device and the server is stable, and there is no retransmission needed. Each layer introduces DP and CP overhead of 10% and 5%, respectively. Furthermore, normalization is utilized as the data transformation procedure, as discussed in Section V. Finally, model training requires 10 epochs ( $N_{\text{epochs}} = 10$ ) and utilizes 5-fold validation. The energy consumption of this example is shown in Table IV and reveals the contribution of each component to the total energy cost of developing models. Specifically, data collection dominates the total energy cost for developing a very simple model based on a 3-layer, 10-nodes-per-layer MLP architecture. For the same parameters, the relative contribution of the data collection decreases for the KAN, CNN and transformer architectures, making the energy cost of training the primary contributor. The eCAL calculator enables changing the hyperparameters of the four architectures while also adding well known CNN architectures such as ResNets [53], VGGs [54] or transformer-based such as Baichuan 2 [55].

To complement Table IV and provide a more comprehensive energy profile beyond the analysis in Section IV, Fig. 11 shows the energy consumption breakdown that also includes wired portions of the network including fronthaul and backhaul, by using the microcell splits reported in [56]. We examine three fronthaul/backhaul combinations, i.e. Fiber/Fiber, Copper/Radio, and Copper/Fiber to illustrate how the energy mix shifts when wired paths dominate. For computationally light models such as a relatively shallow MLP, deployment energy is no longer dominated by radio access network (RAN)-based data collection as in Table IV; the wired infrastructure becomes the primary contributor, reaching roughly 90% of the total in the Fiber/Fiber case. For complex models such as the simple transformer considered in this work, training

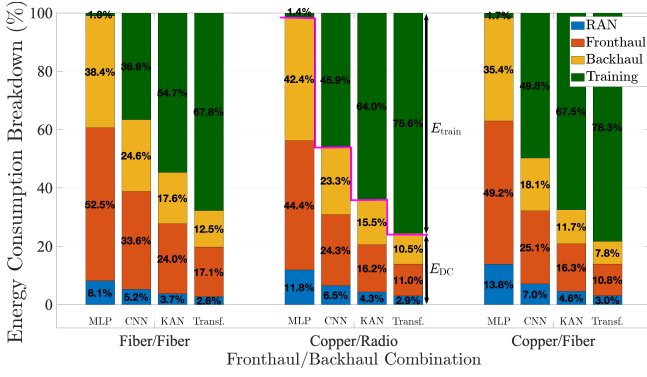


Fig. 11: Comparison of energy consumption of training ( $E_{\text{train}}$ , highlighted in upper part of the bars) and data collection ( $E_{\text{DC}}$ , highlighted in lower part of the bars, divided into three parts: RAN, Fronthaul, and Backhaul for different models in different Fronthaul/Backhaul combinations.

remains the largest single component in energy consumption, but its share drops markedly once wired costs are included, which falling from over 96% in the wireless-only view from Table IV to approximately 68–78% across the three scenarios as depicted in Fig. 11. Importantly, the underlying absolute energies (in Joules) are unchanged: we add fronthaul and backhaul (derived from the microcell splits) to the per-model totals and then recompute percentage shares. The RAN data-collection energy is exactly the same as in Table IV. Taken together, these results show a holistic energy assessment in modern hybrid networks, and emphasize the flexibility of the eCAL framework in modeling diverse scenarios.

Once the model is developed, it is packaged and deployed in the communication system, where it can produce inference in the form of continuous or discrete outputs. During its operational lifecycle, the model will be presented with input data and requested to produce the corresponding inference. Thus, we can express the associated energy cost as follows:

$$E_{\text{inf},p} = E_{\text{DC}} + E_{\text{pre}} + E_{\text{inf}}. \quad (28)$$

This means that we consider the energy cost of inference before the current model needs to be updated. The corresponding energy per bit of inference, once deployed, is calculated as follows:

$$E_{\text{inf},p,b} = \frac{E_{\text{inf},p}}{fN_{I,P}I_S}. \quad (29)$$

Next, we calculate the total energy cost over the lifetime of an AI model in the system, also referred to as  $eCAL_{\text{abs}}$  (measured in  $[J]$ ). It is defined as the sum of energy consumed during the model development,  $E_{\text{D}}$  and the energy required for performing an inference  $E_{\text{inf},p}$ , multiplied by the number of times  $\gamma \in [0, \infty)$  the inference is performed with the currently deployed model. In addition, as edge cloud systems may use virtualization in developing and operating the models, we enable considering the impact of such technologies through an additional factor. As a result,  $eCAL_{\text{abs}}$  can be expressed as:

$$eCAL_{\text{abs}} = (1 + \gamma_v) (E_{\text{D}} + \gamma E_{\text{inf},p}), \quad (30)$$

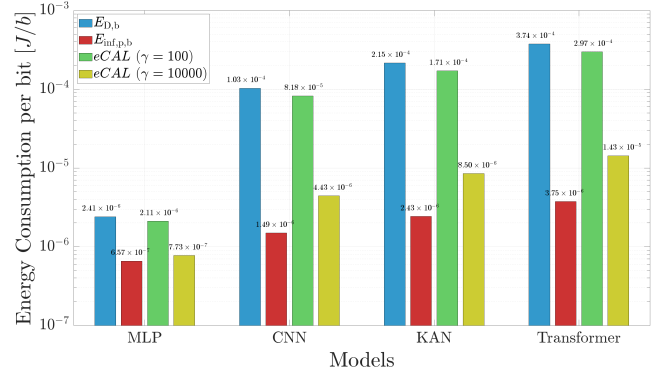


Fig. 12: Comparison of energy consumption per bit in different data manipulation components over the lifecycle of the AI model.

where  $\gamma_v$  represents the contribution from the virtualization, with  $\gamma_v = 0$  corresponding to no virtualization. The reason for simplifying the estimation of the overhead introduced by the virtualization technologies in eCAL through a factor  $\gamma_v$  is that the virtualization technologies in cloud systems are relatively well established while in communication systems they are still emerging. Furthermore, they depend on the configuration of the cloud-edge virtualization (e.g. bare-metal vs containers) and platform stacks (e.g. K8s vs K3s vs MicroK8s) as well as MLOps technology stack selection. For instance, there is significant difference in control-plane overhead on the platform layer of the CCRA depending on the number of control plane and worker plane nodes across K8s versions as shown in [57]. Furthermore, there is significant overhead difference between the standard O-RAN MLOps stack vs. NAOMI, a recently introduced distributed alternative [58]. In the future, as technologies will mature and consolidate, it is possible to set this factor to 0, tune the overhead in Eqs. (2) and incorporate compute and control plane overhead in Eq. (30) to enable more fine grained analytical study of virtualization impact.

Finally, the proposed eCAL metric computing the corresponding energy consumption per bit over the lifecycle of the currently deployed AI model can be expressed as:

$$eCAL = \frac{eCAL_{\text{abs}}}{fI_S(N_S + \gamma N_{I,P})}. \quad (31)$$

To further quantify this relationship, we first compare the outcomes of Eqs. (27), (29) and (31), depicted in Fig. 12. The figure shows that the energy consumption per bit of developing a 3 layer - 10 node MLP is  $2.41 \times 10^{-6} [J/b]$ , which is approximately 3.7 times higher than the energy consumption per bit of one inference ( $E_{\text{inf},p,b} = 6.57 \times 10^{-7} [J/b]$ ). Furthermore, we can observe that the energy consumption per bit decreases with more inferences, dropping from  $2.11 \times 10^{-6} [J/b]$  for 100 inferences to  $7.73 \times 10^{-7} [J/b]$  for 1000 inferences, which is a 2.73 times of improvement on energy efficiency. Moreover, we can observe that models with architectural blocks that require higher computational complexity need significantly more energy per bit during development compared to simpler models and their energy cost per bit of one inference. For

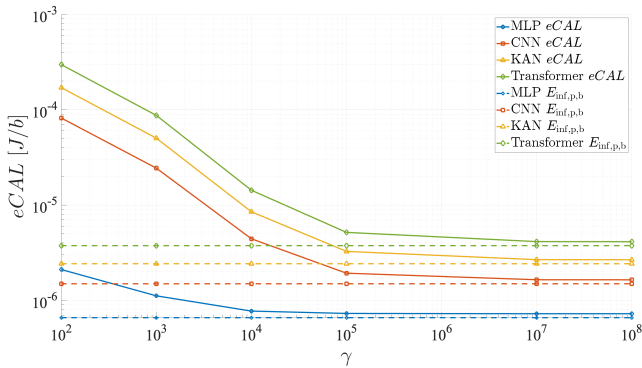


Fig. 13: Energy cost of AI model lifecycle ( $eCAL$ ) for different models over the number of inferences ( $\gamma$ ), log scale on both axes.

instance, the transformer consumes  $3.74 \times 10^{-4}$  [J/b], which means it is nearly 165 and 20.7 times less energy efficient per bit than the MLP in making 100 and 1000 inferences, respectively. Fig. 13 further confirms that as the number of inferences  $\gamma$  in the current model increases, the EE of the AI model lifecycle improves.

*Implementation guidelines:* The open-source  $eCAL$  calculator (Python), can be used standalone to compute  $eCAL$  values using provided configuration files. Users can study custom scenarios, such as different transmit powers, overheads, or neural network configurations by editing these files. Thanks to its modular design, new protocols or neural architectures can be added via dedicated class implementations. Python-based simulators can integrate it directly by importing its functionality, while other simulators may require minor additional development.

## IX. CONCLUSIONS AND FUTURE WORK

In this work, we have proposed a novel metric, namely,  $eCAL$ . Unlike traditional metrics that focus only on energy required for transmission, computing infrastructure, or AI models separately,  $eCAL$  can capture the overall energy cost of generating inferences in communication system during the entire lifecycle of a trained model. We have proposed a detailed methodology to determine the  $eCAL$  of an AI enhanced communication system by breaking it down into various data manipulation components, such as data collection, preprocessing, training, evaluation, and inference, and analyzing the complexity and energy consumption of each component. The proposed metric demonstrates that the more a model is utilized, the more energy-efficient each inference becomes. For example, considering a simple MLP architecture, the energy consumption per bit for 100 inferences is 2.73 times higher than for 1000 inferences. Based on the proposed methodology we also developed an open-source, modular  $eCAL$  calculator which enables fine-grained analysis of energy consumption across components, allowing developers to evaluate and optimize AI EE in various deployment scenarios.

Through the proposed  $eCAL$  metric, this study lays the foundation for understanding the energy consumption of AI-

enhanced emerging communication architectures. Future work may focus on extending this work beyond the assumptions, case studies, and configurations provided in this paper to cover existing and emerging communication system designs that are increasingly relying on AI techniques for their automation and performance optimization, especially the emerging open radio access network (O-RAN) based cellular systems and caching mechanism. The exploration of the relationship between model performance and  $eCAL$  for 6G verticals, related network slices, online, distributed, fine tuned and federated model lifecycles may also be worthy of pursuing. Finally, the development of dynamic energy management algorithms in view of a more sustainable operation is highly relevant.

*Acknowledgements:* This work was supported in part by the HORIZON-MSCA-PF project TimeSmart (No. 101063721), the European Commission NANCY project (No. 101096456), and the Slovenian Research Agency under grants P2-0016, MN-0009-106, and J2-50071.

## REFERENCES

- [1] K. B. Letaief, W. Chen, Y. Shi, J. Zhang, and Y.-J. A. Zhang, "The roadmap to 6G: AI empowered wireless networks," *IEEE Commun. Mag.*, vol. 57, no. 8, pp. 84–90, 2019.
- [2] J. Hoydis, F. A. Aoudia, A. Valcarce, and H. Viswanathan, "Toward a 6G AI-native air interface," *IEEE Commun. Mag.*, vol. 59, no. 5, pp. 76–81, 2021.
- [3] W. Wu, C. Zhou, M. Li, H. Wu, H. Zhou, N. Zhang, X. S. Shen, and W. Zhuang, "AI-native network slicing for 6G networks," *IEEE Wireless Commun.*, vol. 29, no. 1, pp. 96–103, 2022.
- [4] Y. Huang, X. You, H. Zhan, S. He, N. Fu, and W. Xu, "Learning wireless data knowledge graph for green intelligent communications: Methodology and experiments," *IEEE Trans. Mobile Comput.*, vol. 23, no. 12, pp. 12 298–12 312, 2024.
- [5] C. Chaccour, W. Saad, M. Debbah, Z. Han, and H. Vincent Poor, "Less data, more knowledge: Building next-generation semantic communication networks," *IEEE Communications Surveys & Tutorials*, vol. 27, no. 1, pp. 37–76, 2025.
- [6] A. R. Hossain, W. Liu, N. Ansari, A. Kiani, and T. Saboorian, "AI-native end-to-end network slicing for next-generation mission-critical services," *IEEE Trans. Cogn. Commun. Netw.*, vol. 11, no. 1, pp. 48–58, 2025.
- [7] O.-R. Alliance, "O-RAN working group 2 AI/ML workflow description and requirements," *ORAN-WG2. AIML. v01.03*, July 2021.
- [8] P. Dhar, "The carbon impact of artificial intelligence," *Nature Machine Intelligence*, vol. 2, no. 8, pp. 423–425, 2020.
- [9] A. S. Luccioni, S. Viguier, and A.-L. Ligozat, "Estimating the carbon footprint of bloom, a 176B parameter language model," *J. Mach. Learn. Res.*, vol. 24, no. 253, pp. 1–15, 2023.
- [10] G. Kamiya, P. Bertoldi *et al.*, *Energy consumption in data centres and broadband communication networks in the EU*. Publications Office of the European Union, 2024.
- [11] E. Garcia-Martín, C. F. Rodrigues, G. Riley, and H. Grahn, "Estimation of energy consumption in machine learning," *Journal of Parallel and Distributed Computing*, vol. 134, pp. 75–88, 2019. [Online]. Available: <https://www.sciencedirect.com/science/article/pii/S0743731518308773>
- [12] A. Luccioni, A. Lacoste, and V. Schmidt, "Estimating carbon emissions of artificial intelligence," *IEEE Technol. Soc. Mag.*, vol. 39, no. 2, pp. 48–51, 2020.
- [13] A. Faiz, S. Kaneda, R. Wang, R. C. Osi, P. Sharma, F. Chen, and L. Jiang, "LLMCarbon: Modeling the end-to-end carbon footprint of large language models," in *Proc. The 12th ICLR*, 2024. [Online]. Available: <https://openreview.net/forum?id=aIok3ZD9to>
- [14] C.-J. Wu, B. Acun, R. Raghavendra, and K. Hazelwood, "Beyond efficiency: Scaling AI sustainably," *IEEE Micro*, 2024.
- [15] P. Zhang, Y. Xiao, Y. Li, X. Ge, G. Shi, and Y. Yang, "Toward net-zero carbon emissions in network AI for 6G and beyond," *IEEE Commun. Mag.*, vol. 62, no. 4, pp. 58–64, Apr. 2024.

- [16] S. Savazzi, V. Rampa, S. Kianoush, and M. Bennis, "An energy and carbon footprint analysis of distributed and federated learning," *IEEE Trans. Green Commun. Netw.*, vol. 7, no. 1, pp. 248–264, Mar. 2023.
- [17] X. Hou, J. Liu, X. Tang, C. Li, J. Chen, L. Liang, K.-T. Cheng, and M. Guo, "Architecting efficient multi-modal AIoT systems," in *Proc. 50th Annual International Symposium on Computer Architecture*. New York, USA: Association for Computing Machinery, Jun. 2023. [Online]. Available: <https://doi.org/10.1145/3579371.3589066>
- [18] S. Zhu, K. Ota, and M. Dong, "Energy-efficient artificial intelligence of things with intelligent edge," *IEEE Internet of Things J.*, vol. 9, no. 10, pp. 7525–7532, May 2022.
- [19] B. Bertalanič, M. Meža, and C. Fortuna, "Resource-aware time series imaging classification for wireless link layer anomalies," *IEEE Trans. Neural Netw. Learn. Syst.*, vol. 34, no. 10, pp. 8031–8043, 2022.
- [20] D. Trihinas, L. Thamsen, J. Beilharz, and M. Symeonides, "Towards energy consumption and carbon footprint testing for AI-driven IoT services," in *Proc. IEEE IC2E*, Sept. 2022, pp. 29–35.
- [21] C. Naastepad and F. Com, "Labour market flexibility, productivity and national economic performance in five European economies," *Dutch Report, Flexibility and Competitiveness: Labour Market Flexibility, Innovation and Organisation Performance*, EU Commission DG Research Contract HPSE-CT-2001-00093, 2003.
- [22] P. Rysavy, "Challenges and considerations in defining spectrum efficiency," *Proceedings of the IEEE*, vol. 102, no. 3, pp. 386–392, 2014.
- [23] J. Buberger, A. Kersten, M. Kuder, R. Eckerle, T. Weyh, and T. Thiringer, "Total CO<sub>2</sub>-equivalent life-cycle emissions from commercially available passenger cars," *Renewable and Sustainable Energy Reviews*, vol. 159, p. 112158, 2022. [Online]. Available: <https://www.sciencedirect.com/science/article/pii/S1364032122000867>
- [24] J. Diaz-De-Arcaya, A. I. Torre-Bastida, G. Zárate, R. Miñón, and A. Almeida, "A joint study of the challenges, opportunities, and roadmap of mlops and AIops: A systematic survey," *ACM Computing Surveys*, vol. 56, no. 4, pp. 1–30, 2023.
- [25] D. Barry, A. Danalis, and H. Jagode, "Effortless monitoring of arithmetic intensity with papi's counter analysis toolkit," in *Proc. Tools for High Performance Computing 2018/2019*. Springer, 2021, pp. 195–218.
- [26] R. Pereira, M. Couto, F. Ribeiro, R. Rua, J. Cunha, J. P. Fernandes, and J. Saraiva, "Ranking programming languages by energy efficiency," *Science of Computer Programming*, vol. 205, p. 102609, 2021.
- [27] H. R. Chi, A. Radwan, C. Zhang, and A.-E. M. Taha, "Managing energy-experience trade-off with AI towards 6G vehicular networks," *IEEE Communications Standards Magazine*, vol. 7, no. 3, pp. 24–31, 2023.
- [28] P. Pegus, B. Varghese, T. Guo, D. Irwin, P. Shenoy, A. Mahanti, J. Culbert, J. Goodhue, and C. Hill, "Analyzing the efficiency of a green university data center," in *Proceedings of the 7th ACM/SPEC on International Conference on Performance Engineering*, ser. ICPE '16. New York, NY, USA: Association for Computing Machinery, 2016, p. 63–73. [Online]. Available: <https://doi.org/10.1145/2851553.2851557>
- [29] S. L. Jurj, F. Opritoiu, and M. Vladutiu, "Environmentally-friendly metrics for evaluating the performance of deep learning models and systems," in *Proc. ICONIP*. Springer, 2020, pp. 232–244.
- [30] R. Bolla, R. Bruschi, O. M. Jaramillo Ortiz, and P. Lago, "The energy consumption of tcp," in *Proceedings of the Fourth International Conference on Future Energy Systems*, ser. e-Energy '13. New York, NY, USA: Association for Computing Machinery, 2013, p. 203–212. [Online]. Available: <https://doi.org/10.1145/2487166.2487189>
- [31] T. Stefanec and M. Kusek, "Comparing energy consumption of application layer protocols on IoT devices," in *2021 16th International Conference on Telecommunications (ConTEL)*, 2021, pp. 23–28.
- [32] J. Schandy, L. Steinfeld, and F. Silveira, "Average power consumption breakdown of wireless sensor network nodes using ipv6 over Ilns," in *2015 International Conference on Distributed Computing in Sensor Systems*, 2015, pp. 242–247.
- [33] N. Drucker, S. Gueron, and V. Krasnov, "Making aes great again: The forthcoming vectorized aes instruction," in *16th International Conference on Information Technology-New Generations (ITNG 2019)*, S. Latifi, Ed. Cham: Springer International Publishing, 2019, pp. 37–41.
- [34] R. Liu and N. Choi, "A first look at wi-fi 6 in action: Throughput, latency, energy efficiency, and security," *Proc. ACM Meas. Anal. Comput. Syst.*, vol. 7, no. 1, mar 2023. [Online]. Available: <https://doi.org/10.1145/3579451>
- [35] H. Schippers, M. Geis, S. Böcker, and C. Wietfeld, "DoNext: An open-access measurement dataset for machine learning-driven 5G mobile network analysis," *IEEE trans. mach. learn. commun. netw.*, vol. 3, pp. 585–604, apr 2025.
- [36] Arm Ltd., "ArmV8 cryptography extensions," <https://developer.arm.com/documentation/>, 2013, overview and performance guidance for AES-GCM on ArmV8 Crypto Extensions.
- [37] OpenSSL Project, "Openssl speed benchmark documentation," <https://www.openssl.org/docs/>, ongoing, empirical AES-GCM throughput used as a practical reference.
- [38] Intel Corporation, "Intel® advanced encryption standard (aes) new instructions set," <https://www.intel.com/>, 2010, white paper and programming references for AES-NI performance.
- [39] —, "Intel architecture instruction set extensions and future features programming reference," <https://www.intel.com/>, 2020, vAES (vector AES) via AVX-512; guidance on multi-block AES throughput.
- [40] M. Horowitz, "1.1 computing's energy problem (and what we can do about it)," in *IEEE International Solid-State Circuits Conference (ISSCC)*, 2014, pp. 10–14.
- [41] N. Javaid, A. Sher, H. Nasir, and N. Guizani, "Intelligence in IoT-based 5G networks: Opportunities and challenges," *IEEE Commun. Mag.*, vol. 56, no. 10, pp. 94–100, Oct. 2018.
- [42] J. Farfan and A. Lohrmann, "Gone with the clouds: Estimating the electricity and water footprint of digital data services in Europe," *Energy Conversion and Management*, vol. 290, p. 117225, 2023. [Online]. Available: <https://www.sciencedirect.com/science/article/pii/S019689042300571X>
- [43] Z. Wang and T. Oates, "Imaging time-series to improve classification and imputation," in *Proceedings of the 24th International Conference on Artificial Intelligence*, ser. IJCAI'15. AAAI Press, 2015, p. 3939–3945.
- [44] K. O'Shea and R. Nash, "An introduction to convolutional neural networks," 2015. [Online]. Available: <https://arxiv.org/abs/1511.08458>
- [45] Z. Liu, Y. Wang, S. Vaidya, F. Ruehle, J. Halverson, M. Soljačić, T. Y. Hou, and M. Tegmark, "Kan: Kolmogorov-arnold networks," 2024. [Online]. Available: <https://arxiv.org/abs/2404.19756>
- [46] A. Vaswani, N. Shazeer, N. Parmar, J. Uszkoreit, L. Jones, A. N. Gomez, Ł. Kaiser, and I. Polosukhin, "Attention is all you need," *Advances in neural information processing systems*, vol. 30, 2017.
- [47] B. Bertalanič and C. Fortuna, "Carmel: Capturing spatio-temporal correlations via time-series sub-window imaging for home appliance classification," *Engineering Applications of Artificial Intelligence*, vol. 127, p. 107318, 2024.
- [48] R. Yu, W. Yu, and X. Wang, "Kan or mlp: A fairer comparison," 2024. [Online]. Available: <https://arxiv.org/abs/2407.16674>
- [49] A. Ouyang, "Understanding the performance of transformer inference," Ph.D. dissertation, Massachusetts Institute of Technology, 2023.
- [50] A. G. Baydin, B. A. Pearlmutter, A. A. Radul, and J. M. Siskind, "Automatic differentiation in machine learning: a survey," *Journal of Machine Learning Research*, vol. 18, no. 153, pp. 1–43, 2018. [Online]. Available: <http://jmlr.org/papers/v18/17-468.html>
- [51] P. Pathania, N. Bamby, R. Mehra, S. Sikand, V. S. Sharma, V. Kaulgud, S. Podder, and A. P. Burden, "Calculating software's energy use and carbon emissions: A survey of the state of art, challenges, and the way ahead," *arXiv preprint arXiv:2506.09683*, 2025.
- [52] A. Pirnat, B. Bertalanič, G. Cerar, M. Mohorčič, M. Meža, and C. Fortuna, "Towards sustainable deep learning for wireless fingerprinting localization," in *ICC 2022 - IEEE International Conference on Communications*, 2022, pp. 3208–3213.
- [53] K. He, X. Zhang, S. Ren, and J. Sun, "Deep residual learning for image recognition," in *2016 IEEE Conference on Computer Vision and Pattern Recognition (CVPR)*, 2016, pp. 770–778.
- [54] K. Simonyan, "Very deep convolutional networks for large-scale image recognition," *arXiv preprint arXiv:1409.1556*, 2014.
- [55] A. Yang, B. Xiao, B. Wang, B. Zhang, C. Bian, C. Yin, C. Lv, D. Pan, D. Wang, D. Yan *et al.*, "Baichuan 2: Open large-scale language models," *arXiv preprint arXiv:2309.10305*, 2023.
- [56] Politecnico di Milano, "Energy Efficiency of Fiber on Mobile Networks," Europacable, Tech. Rep., Dec. 2021, prepared for Europacable.
- [57] D. Mušić, J. Hribar, and C. Fortuna, "Digital transformation with a lightweight on-premise paas," *Future Generation Computer Systems*, vol. 160, pp. 619–629, 2024. [Online]. Available: <https://www.sciencedirect.com/science/article/pii/S0167739X24003261>
- [58] A. Čop, B. Bertalanič, and C. Fortuna, "An overview and solution for democratizing ai workflows at the network edge," *Journal of Network and Computer Applications*, vol. 239, p. 104180, 2025. [Online]. Available: <https://www.sciencedirect.com/science/article/pii/S1084804525000773>